A Low-cost Portable Photoacoustic Breast Cancer Imaging System

Abstract

Summary: Photoacoustic effect is under the spotlight in medical imaging in recent years for its capability to produce images with higher resolution while minimizing the side effects. Many pieces of research are dedicated to transforming the principle into practice. Currently, low-cost portable devices based on the photoacoustic effect are being developed. Here we present a low-cost portable breast cancer imaging system prototype with a light emitting diode as the light source. In this passage, we summarized the mathematical layout of photoacoustic effect-based imaging system design and concluded subsequent codes to follow. Respectively, the key parameters to heed for the light source are the wavelength, pulse duration, the single pulse energy, and the repetition rate. The spatial distribution and the sensitivity distribution function should be considered when selecting transducers. The

Finally, we designed a prototype device in the workflow we proposed.
(The parameters of our device)

We hope our work can demonstrate a systematic approach toward photoacoustic effect-based imaging system design.

Keywords: Breast Cancer, Photoacoustic Imaging, Light Emitting Diode, Photoacoustic Tomography,

Contents

1. Introduction

1.1 Overview

Being discovered in the 1880s, the significance of the photoacoustic effect wasn't recognized until the past few decades.[1] The photoacoustic effect describes the phenomenon that acoustic waves form from thermal expansion when the material absorbs intensity-varying light, and the intensity of the acoustic waves is dependent on the intensity of the light.[2,3] Based on this principle, photoacoustic imaging obtains deeper imaging depth than light-based imaging methods for it utilizes acoustic waves, evading the pitfall of light scattering.[4] Moreover, using light enables photoacoustic imaging to distinguish diverse soft tissue structures, which is the dominant source of error in ultrasonic-based imaging.[5] Although mammography accompanied by ultrasound and MRI are the mainstream methods of cancer screening and inspection, MRI is expensive and brings side effects including radiation and a certain degree of discomfort.[6,7] Besides, mammogram shows inadequacy in women with dense breast tissue, and MRI is criticized for requiring Gadolinium as a contrast agent, which shows a pernicious effect on the human.[8–10]

To reduce or eliminate the defects mentioned above, many pieces of research are centered around photoacoustic imaging. By the scales of measurement, photoacoustic imaging can be categorized into macroscopic imaging, mesoscopic imaging, and microscopic imaging, ranging from organelles to organs.[3,11] We here only focus on macroscopic imaging because our purpose is to develop a system for breast cancer inspection.

Currently, some prototypes of photoacoustic imaging systems have been developed. Of all the imaging systems, a single-breath-hold PACT system shows promise in clinical use, for it reached a penetration depth of 40mm while limiting the scanning time within a single breath hold time, eliminating the disturbance of heartbeat and body movement.[12] A 3D photoacoustic breast imaging system developed by Kruger et al. reached 53mm penetration depth and is approved by the FDA.[13] LOUISA-3D developed by Alexander et al. reached 0.3mm resolution.[13] The multiple measurements combined systems are also under investigation. For instance, the combination of ultrasound tomography, photoacoustic tomography, and thermoacoustic tomography may be applicable for sentinel lymph node imaging and small animal imaging.[14,15]

However, all the above systems use lasers with different wavelengths as the light source, which corresponds to huge expenditure and lack of mobility. More than that, the use of lasers induces safety problems. When designing the device, the safety of laser use should be considered and must abide by the safety code formulated by IEEE.[12] Some shreds of evidence suggest that alternative sources of light may be possible. The two main alternative light sources are light emitting diodes and pulsed laser diodes. Li et al. developed a photoacoustic imaging system based on a blue-ray DVD, reaching 1 μm in lateral resolution and 225 μm in penetration depth.[16] The imaging system developed by Zeng et al. using LED reached a lateral resolution of 0.95 μm and an SNR of 38 dB.[17] Elaboration of the system setup can be found in the citation here.[18–21] Of note, due to the limitation in pulse energy, the penetration depth using the alternative light sources is compromised.

From the above introduction, we can conclude that the photoacoustic effect plays a promising role in the biomedical field. Set the applications around breast cancer aside, photoacoustic-based system prototypes are of significant use in vascular imaging, joint inflammation detection, and lesion tooth scanning.[21–23] Besides its biomedical applications, the photoacoustic effect casts light on other disciplines. For instance, photoacoustic imaging is applied to recognize the hidden patterns or sketches in oil paintings as well as sculptures.[24,25] By recognizing the ability that the photoacoustic effect possesses, we may apply this technology to other circumstances requiring high resolution and deep penetration depth at the same time.

1.2 Physical Process

We here explain the physical process of the photoacoustic effect and the imaging process briefly and the details will be discussed in later sections. The physical process of the photoacoustic effect includes the absorption of light, the concomitantly rise in temperature, and finally the thermoelastic expansion, resulting in the emission of acoustic waves.[26,27] The eventual purpose is to form images with high resolution as well as contrast. To achieve this, we have to analyze the process with a more rigorous mathematical model. Currently, many mathematical models have been proposed to reflect the physical process as accurately as possible. Peter et al. provided a mathematical overview perspective on photoacoustic tomography.[28] Poudel et al. summarized a computational framework for photoacoustic imaging.[29] Xu et al. proposed the universal back projection method, which serves as the framework of many following models.[30]

Thanks to the dedicated researchers, some algorithms are made open source, which can be found online. For instance, SIMPA is a toolkit for simulation and image processing for photonics and acoustics.[31] MSOT provides a tool for initial pressure image reconstruction.[32] SIGOAT

introduced a "Style Network" to reduce the domain gap between simulated and experimental optoacoustic data.[33] A review of sampling and signal processing summarized current approaches to increasing the contrast and resolution of the images.[34]

In the following sections, we are going to break down the physical process of the photoacoustic effect in *Section 2*, to provide a design framework for our device. Then we make a simulation accordingly in *Section 3*. Finally, we present our design and experiment results in *Section 4*, *Section 5* respectively.

2. Principles Toward Design

We break down photoacoustic imaging into 3 major processes, (1). the emitting of the light source and thermoelastic expansion, (2). acoustic wave propagation, (3). sampling and image processing. Table 1 contains the notations used below and their interpretations.

Table 1

Notation	Interpretation
$\vec{\boldsymbol{r}}$	The position vector
ε_A	The molar extinction coefficient of the chemical A
μ_a	The absorption coefficient
λ	The wavelength
$[A]$	The molar concentration of the chemical A
d_c	The desired spatial resolution of the image
D_T	The thermal diffusivity of the illuminated tissue
v_s	The speed of sound
τ	The pulse duration of the light source
κ	The isothermal compressibility of the illuminated tissue
β	The thermal coefficient of volume expansion
T	The local change in temperature
p	The local change in pressure
ρ	The local mass density of the illuminated tissue
C_V	The specific heat capacity at constant volume
A_e	The absorbed energy density
F	The local optical influence (laser fluency)
Γ	The local Grueneisen parameter
E	The single pulse energy of the light source
f_P	The repetition rate of the light source
d_{il}	The diameter of the illumination region
N	The number of pulses at each illuminating spot
Δ	The scanning step size
k	The interested chromophore number
K	The total number of the interested chromophores
μ_{a-k}	The molar absorption coefficient spectra of an interested chromophore
μ_s	The optical scattering coefficient
C_P	The isobaric specific heat
A	The local heat energy density
h	The impulse response of the transducer
S	The sensitivity distribution of the transducer
$\overrightarrow{\boldsymbol{r_n}}$	The position vector of the n-th transducer
N	The total number of the transducers
ϕ	The local light radiance
$\hat{\boldsymbol{s}}$	A directional vector in R^3
g	The local anisotropy factor
ω_c	The cutoff frequency

2.1 Light Source Emitting and Thermoelastic Expansion

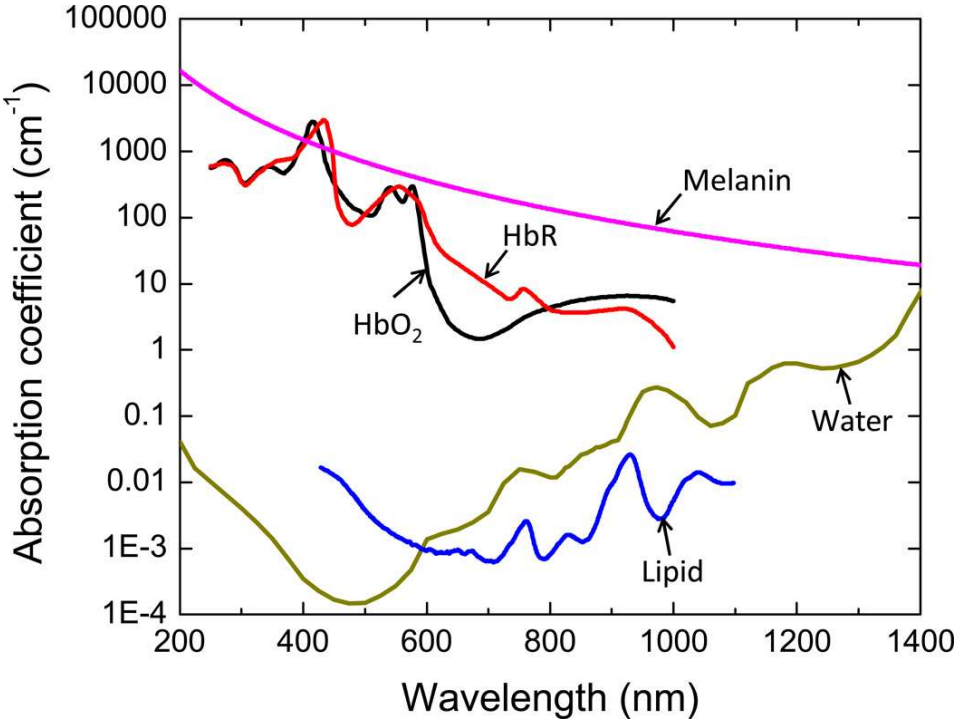

Figure 1

Figure 1. The spectrum of the absorption coefficient of typical endogenous chromophores, including melanin (pink), oxy-hemoglobin (black), deoxy-hemoglobin (red), water (green), and lipid (blue). This figure is retrieved from the citation here[2] and the data is double-checked from its original website.[35]

We recognize the photoacoustic effect takes place only when the light source provides the pulsed light.[1] The key to obtaining a higher contrast on the image, is to amplify the differences among tissues. As is depicted in **Figure 1**, different wavelengths correspond to different absorption values of chromophores.[35] By selecting distinctive wavelengths for the light source, we are able to reach a higher level of contrast. What's more, the use of contrast agents can improve the image contrast significantly according to several pilot experiments.[36,37] In addition, the result posted online shows that the absorption rate of blood satisfies the following equation.[35]

$$\mu_a(\vec{r},\lambda) = 2.303 \times \left[\varepsilon_{Hb}(\lambda)\cdot[\mathrm{Hb}](\vec{r}) + \varepsilon_{HbO_2}(\lambda)\cdot[\mathrm{HbO_2}](\vec{r})\right] \tag{1}$$

Before we proceed, there are certain constraints to consider, the thermal confinement threshold and the stress confinement threshold.[27,38] Respectively, they represent the thermal diffusion effect and the volume expansion effect while illuminated by the light, as shown below.

$$\tau < \frac{d_c^2}{4\cdot D_T} \tag{2}$$

$$\tau < \frac{d_c}{v_s} \tag{3}$$

When the pulse duration of the light satisfies the above equations, we can ignore the effect introduced by thermal diffusion and volume expansion, i.e. in *Formula 4*, the left-hand side terms can be set to 0 with confidence. As the pulse duration decreases, the resolution of the image is enhanced.

$$\frac{dV}{V} = -\kappa\cdot p(\vec{r}) + \beta\cdot T(\vec{r}) \tag{4}$$

Refactoring *Formula 4*, we get

$$p(\vec{r}) = \frac{\beta}{\kappa}T(\vec{r}) \tag{5}$$

Using the optical absorption to simplify *Formula 5*, we have

$$T(\vec{r}) = \frac{A_e(\vec{r})}{\rho(\vec{r})\cdot C_V(\vec{r})} \tag{6}$$

Also,

$$A_e(\vec{r}) = \mu_a(\vec{r}) \cdot F(\vec{r}) \tag{7}$$

Combining the 3 formulas above, and using the definition of the Grueneisen parameter.[39] Here its physical interpretation is the efficiency of energy conversion.

$$\Gamma(\vec{r}) = \frac{\beta}{\kappa \cdot C_V \cdot \rho(\vec{r})} \tag{8}$$

We obtain

$$p(\vec{r}) = \Gamma(\vec{r}) \cdot \mu_a(\vec{r}) \cdot F(\vec{r}) \tag{9}$$

To get the physical information about the tissue, we are seeking the initial change in local pressure, which we denote by 0 in the subscript. Note that the above formulas are applied to the illuminated tissue, i.e., the acoustic wave source, then

$$p_0(\vec{r}) = p(\vec{r}) = \Gamma(\vec{r}) \cdot \mu_a(\vec{r}) \cdot F(\vec{r}) \tag{10}$$

Although the light source we selected is light emitting diodes, for generality, we discuss the case of safety issues, especially regarding the regulations made by the IEEE as well as ANSI.[12,40] The parameters of the light source must satisfy

$$\mathrm{E} < 20\mathrm{mJ} \tag{11}$$

$$\frac{E}{f_P} < 200\mathrm{mW} \tag{12}$$

Also, according to a review, for raster scanning photoacoustic microscopy in 400-700 nm spectrum, the parameters should satisfy[27]

$$\mathrm{E} \cdot \sqrt[4]{f_P} \leq 2.75 \times 10^2 \times \pi \cdot d_{il}^{\frac{5}{4}} \cdot \left(\frac{\Delta}{N}\right)^{\frac{3}{4}} \tag{13}$$

Later in *Section 2.3*, we will illustrate that as the pulse repetition rate increases, the time required for scanning decreases. To achieve real-time scanning, the pulse repetition rate must be frequent enough.

In summary, for light source selection, certain parameters must be taken into full consideration, including the wavelength (λ), pulse duration (τ), the single pulse energy of the light source (E), and the repetition rate (f_P).

2.2 Light Wave Travelling and Acoustic Wave Propagation

Two problems will be addressed in this section. (1) How does the excitation light propagate within the tissue, i.e., the optical inverse problem, and (2) How does the acoustic wave propagate and interact with the transducers, i.e., the acoustic inverse problem. We discuss them separately because their principles are different. We address them along with the flow of signal. The two problems are interconnected by *Equation (10)*, where $p_0(\vec{r})$ and $\mu_a(\vec{r})$ are respectively the desired result of the two problems.

2.2.1 Acoustic Inverse Problem

As concluded earlier, our purpose is to find the initial local pressure change distribution $p_0(\vec{r})$. However, due to the transmitting time of the signal and limited sampling positions, we can only sample the propagated acoustic wave $p(\vec{r}, \mathrm{t})$. The following procedure is to find $p_0(\vec{r})$ using $p(\vec{r}, \mathrm{t})$ in inverse order, thus the problem of image reconstruction is categorized as an inverse acoustic problem.[30] Along the process, we will discuss the transducers used to collect the propagated wave and the method of scanning.

Firstly, we make a few assumptions for simplicity.

Assumption 1. The tissue is acoustically homogeneous, which can be represented as

$$\Gamma(\vec{r}) = \frac{\beta}{\kappa \cdot C_V \cdot \rho(\vec{r})} = \frac{\beta}{\kappa \cdot C_V \cdot \rho} = \Gamma \tag{14}$$

From *Formula (10)*, by substituting Formula (14), we get

$$p_0(\vec{r}) = \Gamma \cdot \mu_a(\vec{r}) \cdot F(\vec{r}, t) \tag{15}$$

Using Newton's 2nd law, we have the acoustic wave equation[41]

$$\square p(\vec{r}, t) = \frac{\beta}{C_P} \cdot \frac{\partial}{\partial t}[\mu_a(\vec{r}) \cdot F(\vec{r}, t)] \tag{16}$$

Where $\square$ is the d'Alembert operator, which can be expanded as

$$\square = \frac{1}{v_s^2}\frac{\partial^2}{\partial t^2} - \nabla^2 \tag{17}$$

Noting that in thermodynamics, the relationship between specific heat capacity at constant volume and isobaric specific heat abides by the equation[41]

$$\kappa = \frac{C_P}{C_V} \tag{18}$$

Since all the operators involved in the differential equation are integrated into a d'Alembert operator, satisfying the linearity requirement. Using Green's function, the solution to *Equation (16)* is shown below.[42]

$$p_\delta(\vec{r}, t) = \frac{\delta(|\vec{r}| - v_s \cdot t)}{4\pi \cdot |\vec{r}|} \tag{19}$$

Since the differential equation is linear, the superposition principle holds. By superposing all possible locations of the tissue, we get

$$p(\vec{r}, t) = \frac{\Gamma}{4\pi} \int \frac{\delta\left(\left|\vec{r} - \overrightarrow{r'}\right| - v_s \cdot (t - t')\right)}{\left|\vec{r} - \overrightarrow{r'}\right|} \mu_a(\vec{r}) \cdot F(\vec{r}) d\overrightarrow{r'} \mathrm{d}t' \tag{20}$$

As we mentioned in the former section, the pulse duration of the light source satisfies the thermal confinement threshold and the stress confinement threshold. It's proven that by satisfying both confinements, the term $\mu_a(\vec{r}) \cdot F(\vec{r})$ can be approximated.

$$\mu_a(\vec{r}) \cdot F(\vec{r}) \approx A(\vec{r}) \cdot \delta(t) \tag{21}$$

Thus, by substituting *Formula (21)* into *Formula (15)* and *Formula (20)*, we get

$$p_0(\vec{r}) = \Gamma \cdot A(\vec{r}) \tag{22}$$

$$p(\vec{r}, t) = \frac{\Gamma}{4\pi \cdot v_s} \frac{\partial}{\partial t} \int_{\left|\vec{r} - \overrightarrow{r'}\right| = v_s \cdot t} \frac{A(\vec{r})}{\left|\vec{r} - \overrightarrow{r'}\right|} \mathrm{d}\overrightarrow{r'} \tag{23}$$

Now the pressure distribution over the spatial domain and time domain can be solved theoretically. From now on, there are multiple ways to obtain the initial pressure distribution $p_0(\vec{r})$. Here we adopt the categorization proposed by Amir et al. that the acoustic inversion problem can be solved by 4 approaches, namely time-domain algorithms, frequency-domain algorithms, time-reversal algorithms, and model-based algorithms.[43] We discuss the back-projection algorithm in detail for its wide application and excellent reconstruction quality.[44]

To measure the acoustic wave, a sensor named transducer is introduced. Based on the piezoelectric effect, the transducer is able to convert the acoustic signal into an electrical signal.[45] However, the transducer has a limited bandwidth as well as limited resolution, we must take the properties of the transducer into account.[46] We use the subscript *trn* to indicate the transducer. The acoustic signal detected by the transducer satisfies the formula below.[47,48]

$$p_{trn}(\overrightarrow{\boldsymbol{r}_{\boldsymbol{trn}}}, \mathrm{t}) = \mathrm{h(t)} * \int_{S_{trn}} p(\vec{r}, t) \cdot S(\vec{r})\, dS \tag{24}$$

Assume at a specific time t_0, the collected data form a set $\{p_n(\vec{r}, t_0) | n = 1,2, \dots, N\}$. Recalling *Assumption 1*, since v_s is homogeneous, the possible wave source of the collected wave signal is on a spherical shell with a radius equal to $v_s \cdot t_0$. The sphere shell corresponding to the n-th transducer is denoted as S_n. For all transducers, we project the signal onto the corresponding sphere shell, the intersection among sphere shells is the wave source. As is the most common case, we make an assumption that

Assumption 2. The distance between the tissue and the transducer is significantly larger than the size of the tissue. (far-field)[49,50]

Mathematically speaking, we have

$$|\overrightarrow{\boldsymbol{r}_{\boldsymbol{n}}} - \vec{r}| \cong |\overrightarrow{\boldsymbol{r}_{\boldsymbol{n}}}| \tag{25}$$

Then

$$p_{0n}(\vec{r}) = 2 \int_{S_n} \left(\left[p_n(\overrightarrow{\boldsymbol{r}_{\boldsymbol{n}}}, t) - t \cdot \frac{\partial}{\partial t} p_n(\overrightarrow{\boldsymbol{r}_{\boldsymbol{n}}}, t) \right] \middle| \left|\vec{r} - \overrightarrow{r'}\right| = v_s \cdot t \right) \frac{d}{\Omega_0} \Omega_r(\overrightarrow{\boldsymbol{r}_{\boldsymbol{n}}}) \tag{26}$$

$$d\Omega_r(\overrightarrow{\boldsymbol{r}_{\boldsymbol{n}}}) \cong [\widehat{\boldsymbol{r}_{\boldsymbol{n}}} \cdot \vec{\boldsymbol{n}}(\overrightarrow{\boldsymbol{r}_{\boldsymbol{n}}})] \frac{dS}{|\overrightarrow{\boldsymbol{r}_{\boldsymbol{n}}}|^2} \tag{27}$$

Where S denotes the detection surface, $\vec{\boldsymbol{n}}$ denotes the normal vector pointing out the surface, and Ω denotes the solid angle. For different detection surfaces, the corresponding solid angle varies. For instance, when the detection surface is spherical or cylindrical, the solid angle is 4π. Finally, the solution to the inverse acoustic problem is the superposition of each transducer's projection.

Moreover, the related problem in image processing is termed the deconvolution problem.[51] In regard to this particular problem, a lot of algorithms have been implemented, a comprehensive review on photoacoustic imaging can be found in the citation here.[52]

In summary, the projection surface and transducer should be examined when designing a photoacoustic imaging system. More specifically, the spatial distribution ($\overrightarrow{r_n}$) and the sensitivity distribution function of the transducers (S). For certain imaging algorithms, the far-field condition should be satisfied.

2.2.2 Optical Inverse Problem

Since the absorption coefficient is a function of wavelength as shown earlier, we explicitly include wavelength in future discussions. The local absorption coefficient of tissue can be expressed as the linear combination of the absorption coefficient of the interested chromophores weighted by their concentration.

$$\mu_a(\vec{r},\lambda) = \sum_{k=1}^{K} \mu_{a-k}(\lambda)\cdot[k](\vec{r}) \tag{28}$$

Considering the scattering effects and decay effects taking place within the tissue, we conclude that the local optical influence is affected by the absorption coefficient and scattering coefficient.

$$F = F(\vec{r},\lambda;\mu_a,\mu_s) \tag{29}$$

According to a review, two major methods are adopted in solving the optical inverse problem, namely the radiative transfer equation method and the diffusion approximation method.[53] We address them as below.

Since the computation of Maxwell's equations is expensive, we start based on recognizing light as beams composed of photons instead of a wave. Using the radiative transfer equation, we have

$$\frac{1}{v_s}\frac{\partial}{\partial t}\phi(\vec{r},\hat{s},\mathrm{t}) = \mathrm{q}(\vec{r},\hat{s},\mathrm{t}) - [\hat{s}\cdot\nabla + \mu_a(\vec{r}) + \mu_s(\vec{r})]\phi(\vec{r},\hat{s},\mathrm{t}) + \mu_s(\vec{r})\cdot\int \Theta(\hat{s},\hat{s}')\cdot\phi(\vec{r},\hat{s},t)d\hat{s}' \tag{30}$$

(a) (b) (c) (d)

The upper formula is a representation of the law of conservation. It studies how the rate of change of the light radiance changes with respect to spatial position, direction, and time. In the equation, the term (a) represents the total change in the number of photons. Term (b) represents the net flux of the photons as $\mathrm{q}(\vec{r},\hat{s},\mathrm{t})$ is defined as the exogenous change in photon quantity. Term (c) composes of three items, $\hat{s}\cdot\nabla$ represents the photons flowing out due to the gradient, $\mu_a(\vec{r})$ represents the photons absorbed by the tissue, and $\mu_s(\vec{r})$ represents the photons scattered to other directions. The $\Theta(\hat{s},\hat{s}')$ in term (d) is called the scattering phase function. It models the probability of a scattered photon switching traveling direction from $\hat{s}$ to $\hat{s}'$.[54] This term can be interpreted as the scattered photons switching back to the original traveling direction, which contributes to the increase of radiance.

By replacing the time-dependent terms on both sides in *Formula (30)* with the corresponding time-independent terms, we obtain the time-independent radiative transfer equation. The left-hand term is erased since photoacoustic imaging utilizes pulsed light sources, and certain constraints are required to be satisfied, resulting in the compressed pulse duration of the light source, thus for most of the time, $\frac{\partial}{\partial t}\phi(\vec{r},\hat{s},\mathrm{t}) = 0$.

We get

$$[\hat{s}\cdot\nabla + \mu_a(\vec{r}) + \mu_s(\vec{r})]\phi(\vec{r},\hat{s}) - \mu_s(\vec{r})\cdot\int \Theta(\hat{s},\hat{s}')\cdot\phi(\vec{r},\hat{s})d\hat{s}' = \mathrm{q}(\vec{r},\hat{s}) \tag{31}$$

Also, light illumination is the composing effect of the radiance in all directions.

$$\mathrm{F}(\vec{r}) = \int \phi(\vec{r},\hat{s})\,d\hat{s}' \tag{32}$$

By solving Equation (31), we can obtain the local light illumination.[55,56] Since it's difficult to solve most of the time, we introduce the P_N approximation method to obtain the approximation to the radiative transfer function.[57] The definition of the reduced scattering coefficient (μ_s') and optical diffusion coefficient (D) are shown below.

$$\mu_s'(\vec{r}) \coloneqq \big(1-\mathrm{g}(\vec{r})\big)\cdot\mu_s(\vec{r}) \tag{33}$$

$$\mathrm{D}(\vec{r}) = \frac{1}{3\big(\mu_a(\vec{r}) + \mu_s'(\vec{r})\big)} \tag{34}$$

When $\mu_s'(\vec{r}) \gg \mu_a(\vec{r})$, the final analytical expression of $\mathrm{F}(\vec{r})$ using this approximation approach is

$$\mathrm{F}(\vec{\boldsymbol{r}}) = \int \frac{e^{-\mu_{eff}\cdot\left|\vec{\boldsymbol{r}}-\overrightarrow{\boldsymbol{r'}}\right|}}{4\pi\cdot D\cdot\left|\vec{\boldsymbol{r}}-\overrightarrow{\boldsymbol{r'}}\right|}\left(\mu_a(\vec{\boldsymbol{r}})\cdot\mathrm{F}(\vec{\boldsymbol{r}}) + \nabla\cdot\int \hat{\boldsymbol{s}}'\cdot\phi(\vec{\boldsymbol{r}},\hat{\boldsymbol{s}}')d\hat{\boldsymbol{s}}'\right) \tag{35}$$

In which the effective attenuation coefficient

$$\mu_{eff} \coloneqq \sqrt{3\mu_a(\vec{\boldsymbol{r}})\cdot[\mu_a(\vec{\boldsymbol{r}}) + \mu_s'(\vec{\boldsymbol{r}})]} \tag{36}$$

Thus, the absorption coefficient of tissue can be calculated. To obtain the concentration of each interested chromophore, there are multiple ways. Here we discuss the least-square minimization method for its well development. The core of least-square minimization is to locate the errors and try to minimize them. The error function in this context is defined as ε, and the method is shown below.

$$\underset{[k]}{argmin}\ \varepsilon = \frac{1}{2}\left\|\sum_{k=1}^{K}\mu_{a-k}(\lambda)\cdot[k]_{opt}(\vec{\boldsymbol{r}}) - \mu_a(\vec{\boldsymbol{r}},\lambda)\right\|^2 + \mathcal{P}([k]) \tag{37}$$

The subscript for $[k]$ stands for optimization. $\mathcal{P}([k])$ term on the right-hand side represents the penalty function, which is added for special cases. Thus, we obtain the calculated values of $[k]$. Of note, there are many applicable solutions to this problem besides lease-square.[58]

2.3 Signal Processing

After the transducers collected the acoustic signals, the collected signals termed raw data are transported to the data acquisition unit for further processing. One thing should be noted, recalling *Assumption 1* we made, which states that the tissue is acoustically homogeneous for calculation simplicity. However, the acoustical properties of the tissue vary with the speed of sound, tissue density distribution, et cetera, which induces acoustic aberration.[59] This generates sharp edges and reduces resolution in the reconstructed images.[60,61] We address the current solutions in later discussions.

The raw data are the combination of photoacoustic signals and noise. By removing the noise and enhancing the interested signals, we are able to reconstruct the images. The reconstructed images are low in contrast and signal-to-noise ratio, hence the significance of image post-processing.[62,63] We separate our discussions into pre-processing and post-processing since their methodologies are distinct. Here we only discuss the pre-processing step since the post-processing is integrated into the back-projection algorithm.

2.3.1 Pre-processing

The most commonly applied method in pre-processing is averaging.[64] Under the consumption that the ambient noise is uncorrelated random noise, larger averaging times correspond to better convergence. However, there's a tradeoff between accuracy and averaging time, which should be considered when designing real-time photoacoustic imaging systems.[27] By selecting data acquisition units with higher sampling frequency, could this rabbit hole be avoided. The principles are shown below.

Due to the existence of noise, the measured data of the n-th transducer $p_{n-me}(\overrightarrow{\boldsymbol{r_n}},t)$ at time t satisfies

$$p_{n-me}(\overrightarrow{\boldsymbol{r_n}},t) = p_n(\overrightarrow{\boldsymbol{r_n}},t) + z(\overrightarrow{\boldsymbol{r_n}},t) \tag{38}$$

Adopting the assumptions we made above, we illustrate the significance of signal averaging.

Assumption 3. $p_n(\overrightarrow{\boldsymbol{r_n}},t)$ and $z(\overrightarrow{\boldsymbol{r_n}},t)$ are uncorrelated, and $z(\overrightarrow{\boldsymbol{r_n}},t)$ are uncorrelated.

Assumption 4. The noise is random.[65]

Mathematically, they can be expressed as

$$\mathrm{E}[p_n(\overrightarrow{\boldsymbol{r_n}},t)\cdot z(\overrightarrow{\boldsymbol{r_n}},t-\tau)] = 0 \text{ for any } \tau\in\mathrm{R} \tag{39}$$

$$\mathrm{E}[z(\overrightarrow{\boldsymbol{r_n}},t)] = 0 \tag{40}$$

$$\mathrm{D}[z(\overrightarrow{\boldsymbol{r_n}},t)] = \sigma^2 = const \tag{41}$$

The variance of the environmental noise can be expanded as

$$\mathrm{D}[z(\overrightarrow{\boldsymbol{r_n}},t)] = \mathrm{E}[z^2(\overrightarrow{\boldsymbol{r_n}},t)] - E^2[z(\overrightarrow{\boldsymbol{r_n}},t)] = \sigma^2 \tag{42}$$

For total sampling times J, we have

$$\frac{1}{J}\sum_{j=1}^{J}p_{n-me-j}(\overrightarrow{\boldsymbol{r_n}},t) = \frac{1}{J}\sum_{j=1}^{J}p_{n-j}(\overrightarrow{\boldsymbol{r_n}},t) + \frac{1}{J}\sum_{j=1}^{J}z_j(\overrightarrow{\boldsymbol{r_n}},t) \tag{43}$$

By combining the above equations, we obtain the expectation and variance of the averaged signal, which are

$$\mathrm{E}[\bar{p}_{n-me}] = \mathrm{E}\left[\bar{p}_{n-j}(\overrightarrow{\boldsymbol{r_n}}, t)\right] \tag{44}$$

$$\mathrm{D}[\bar{p}_{n-me}] = \mathrm{D}\left[\bar{p}_{n-j}(\overrightarrow{\boldsymbol{r_n}}, t)\right] + \frac{\sigma^2}{J} \tag{45}$$

As J approaches infinity, the last term in *Equation (45)* approaches 0, the noise is reduced, which is the result we desire.[66] When considering the conversion of the analog signals to digital signals, the accuracy and time step length should also be taken into consideration. This step is essential because the collected signals are submerged with the background noise on a large scale.[59]

Another approach is from the frequency perspective, the signal-filtering technique. Using Fourier transformation, the time-domain signals are converted into frequency-domain signals. By selecting cutoff frequencies, the signals whose frequency falls out of the domain can be eliminated. The commonly used filters for signal processing have the problem that the unwanted frequencies are incompletely rejected and the sensitivities for different wavelengths are uneven. Thus, we adopt the Butterworth filter to reach the maximum approximation of uniform sensitivity.[67] The transfer function of an nth-order Butterworth filter is

$$G^2(\omega) = \frac{G_0^2}{1 + (\frac{\omega}{\omega_c})^{2n}} \tag{46}$$

A depiction of a 3-order Butterworth filter is shown in **Figure 2**.

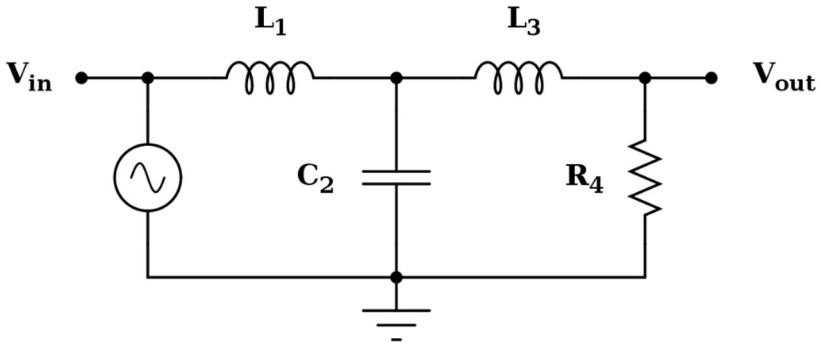

Figure 2

Figure 2. This figure is retrieved from Wikipedia.[68]

Of note, there are multiple sources of noise besides environmental noise, in the form of electronic noise and system thermal noise.[50,62] Different components of the system generate noise of different frequencies. We implemented a virtual Butterworth filter in our algorithm. In summary, the key parameters of the data acquisition unit are sampling frequency, sampling accuracy, and time step length.

3. Simulation

Before diving into the actual building process, we create a simulation to test if our design is reasonable. The methods we are going to apply here are consistent with the methods introduced in the former sections. The data we used are

3.1

4. Design

4.1 Component Selection

Light source

Transducer

(justification)

The details of all the components we purchased can be found in *Table 2*.

Table 2

Component	Serial Number	Manufacture	Price
Total			

Table 2.

4.2 Materials

4.3 Method

4.4 Result

We use

5. Conclusions

In Section

Citations

1. Graham, B. A. The Production of Sound by Radiant Energy. *Science (80-.).* **os-2**, 242–253 (1881).
2. Xia, J., Yao, J. & Wang, L. V. Photoacoustic tomography: principles and advances. *Electromagn. waves (Cambridge, Mass.)* **147**, 1–22 (2014).
3. Wang, L. V & Hu, S. Photoacoustic tomography: in vivo imaging from organelles to organs. *Science* **335**, 1458–1462 (2012).
4. Wang, L., Wu, H.-I. & Masters, B. Biomedical Optics: Principles and Imaging. *J. Biomed. Opt.* **13**, 49902 (2008).
5. Ntziachristos, V. Going deeper than microscopy: the optical imaging frontier in biology. *Nat. Methods* **7**, 603–614 (2010).
6. Lin, E. C. Radiation Risk From Medical Imaging. *Mayo Clin. Proc.* **85**, 1142–1146 (2010).
7. Svahn, T. M., Houssami, N., Sechopoulos, I. & Mattsson, S. Review of radiation dose estimates in digital breast tomosynthesis relative to those in two-view full-field digital mammography. *Breast* **24**, 93–99 (2015).
8. Ibrahim, D., Froberg, B., Wolf, A. & Rusyniak, D. E. Heavy metal poisoning: clinical presentations and pathophysiology. *Clin. Lab. Med.* **26**, 67–97, viii (2006).
9. Murphy, K. J., Brunberg, J. A. & Cohan, R. H. Adverse reactions to gadolinium contrast media: a review of 36 cases. *AJR. Am. J. Roentgenol.* **167**, 847–849 (1996).
10. Pinsky, R. W. & Helvie, M. A. Mammographic breast density: effect on imaging and breast cancer risk. *J. Natl. Compr. Canc. Netw.* **8**, 1157–64; quiz 1165 (2010).
11. Schellenberg, M. W. & Hunt, H. K. Hand-held optoacoustic imaging: A review. *Photoacoustics* **11**, 14–27 (2018).
12. IEEE Standard for Safety Levels with Respect to Human Exposure to Radio Frequency Electromagnetic Fields, 3 kHz to 300 GHz. *IEEE Std C95.1-1991* 1–76 at https://doi.org/10.1109/IEEESTD.1992.101091 (1992).
13. Kruger, R. A. *et al.* Dedicated 3D photoacoustic breast imaging. *Med. Phys.* **40**, 113301 (2013).
14. Ke, H., Liu, C., Wang, L. V, Erpelding, T. N. & Jankovic, L. Performance characterization of an integrated ultrasound, photoacoustic, and thermoacoustic imaging system. *J. Biomed. Opt.* **17**, 1–7 (2012).
15. Reinecke, D. R., Kruger, R. A., Lam, R. B. & DelRio, S. P. Co-registered photoacoustic, thermoacoustic, and ultrasound mouse imaging. in *Proc.SPIE* vol. 7564 (2010).
16. Li, M.-L. & Wang, P.-H. Optical resolution photoacoustic microscopy using a Blu-ray DVD pickup head. in *Proc.SPIE* vol. 8943 (2014).
17. Zeng, L., Piao, Z., Huang, S., Jia, W. & Chen, Z. Label-free optical-resolution photoacoustic microscopy of superficial microvasculature using a compact visible laser diode excitation. *Opt. Express* **23**, 31026–31033 (2015).
18. Erfanzadeh, M. & Zhu, Q. Photoacoustic imaging with low-cost sources; A review. *Photoacoustics* **14**, 1–11 (2019).
19. Rao, A. P., Bokde, N. & Sinha, S. Photoacoustic Imaging for Management of Breast Cancer: A Literature Review and Future Perspectives. *Applied Sciences* vol. 10 at https://doi.org/10.3390/app10030767 (2020).
20. Zhu, Y. *et al.* Light Emitting Diodes based Photoacoustic Imaging and Potential Clinical Applications. *Sci. Rep.* **8**, 9885 (2018).
21. Valluru, K. S. & Willmann, J. K. Clinical photoacoustic imaging of cancer. *Ultrason. (Seoul, Korea)* **35**, 267–280 (2016).
22. Jo, J. *et al.* Detecting joint inflammation by an LED-based photoacoustic imaging system: a feasibility study. *J. Biomed. Opt.* **23**, 1–4 (2018).
23. Pramanik, M. Improving tangential resolution with a modified delay-and-sum reconstruction algorithm in photoacoustic and thermoacoustic tomography. *J. Opt. Soc. Am. A* **31**, 621–627 (2014).
24. Tserevelakis, G. J. *et al.* Photoacoustic imaging reveals hidden underdrawings in paintings. *Sci. Rep.* **7**, 747 (2017).
25. Tserevelakis, G. J. *et al.* Revealing Hidden Features in Multilayered Artworks by Means of an Epi-Illumination Photoacoustic Imaging System. *J. Imaging* **7**, (2021).
26. Neprokin, A., Broadway, C., Myllylä, T., Bykov, A. & Meglinski, I. Photoacoustic Imaging in Biomedicine and Life Sciences. *Life* **12**, (2022).
27. Li, C. & Wang, L. V. Photoacoustic tomography and sensing in biomedicine. *Phys. Med. Biol.* **54**, R59–R97 (2009).
28. KUCHMENT, P. & KUNYANSKY, L. Mathematics of thermoacoustic tomography. *Eur. J. Appl. Math.* **19**, 191–224 (2008).
29. Poudel, J., Lou, Y. & Anastasio, M. A. A survey of computational frameworks for solving the acoustic inverse problem in three-dimensional photoacoustic computed tomography. *Phys. Med. & Biol.* **64**, 14TR01 (2019).

30. Xu, M. & Wang, L. V. Universal back-projection algorithm for photoacoustic computed tomography. *Phys. Rev. E* **71**, 16706 (2005).
31. Gröhl, J. *et al.* SIMPA: an open-source toolkit for simulation and image processing for photonics and acoustics. *J. Biomed. Opt.* **27**, 1–21 (2022).
32. https://github.com/juestellab/mb-rec-msot.
33. Susmelj, A. K. *et al.* Signal Domain Learning Approach for Optoacoustic Image Reconstruction from Limited View Data. *Proceedings of Machine Learning Research-Under Review* 1–19 at (2022).
34. Manwar, R., Zafar, M. & Xu, Q. Signal and Image Processing in Biomedical Photoacoustic Imaging: A Review. *Optics* vol. 2 at https://doi.org/10.3390/opt2010001 (2021).
35. https://omlc.org/index.html.
36. Zhou, Y. *et al.* A Phosphorus Phthalocyanine Formulation with Intense Absorbance at 1000 nm for Deep Optical Imaging. *Theranostics* **6**, 688–697 (2016).
37. Kim, C., Favazza, C. & Wang, L. V. In Vivo Photoacoustic Tomography of Chemicals: High-Resolution Functional and Molecular Optical Imaging at New Depths. *Chem. Rev.* **110**, 2756–2782 (2010).
38. Wang, L. V. Tutorial on Photoacoustic Microscopy and Computed Tomography. *IEEE J. Sel. Top. Quantum Electron.* **14**, 171–179 (2008).
39. Grüneisen, E. Theorie des festen Zustandes einatomiger Elemente. *Ann. Phys.* **344**, 257–306 (1912).
40. Institute, A. N. S. *American national standard for safe use of lasers*. (Laser Institute of America, 2007).
41. Bschorr, O. & Raida, H.-J. Spherical One-Way Wave Equation. *Acoustics* vol. 3 at https://doi.org/10.3390/acoustics3020021 (2021).
42. Sheppard, C. J. R., Kou, S. S. & Lin, J. The Green-function transform and wave propagation . *Frontiers in Physics* vol. 2 at https://www.frontiersin.org/articles/10.3389/fphy.2014.00067 (2014).
43. A., R., V., N. & D., R. Acoustic inversion in optoacoustic tomography: A review. *Current Medical Imaging Reviews* vol. 9 318–336 at http://www.embase.com/search/results?subaction=viewrecord&from=export&id=L372295098%0Ahttp://dx.doi.org/10.2174/15734056113096660006 (2013).
44. Rosenthal, A., Ntziachristos, V. & Razansky, D. Acoustic inversion in optoacoustic tomography: A review. *Curr. Med. Imaging* **9**, 318–336 (2013).
45. Haq, M. Application of piezo transducers in biomedical science for health monitoring and energy harvesting problems. *Mater. Res. Express* **6**, 22002 (2018).
46. Manbachi, A. & Cobbold, R. S. C. Development and Application of Piezoelectric Materials for Ultrasound Generation and Detection. *Ultrasound* **19**, 187–196 (2011).
47. Haltmeier, M. & Zangerl, G. Spatial resolution in photoacoustic tomography: effects of detector size and detector bandwidth. *Inverse Probl.* **26**, 125002 (2010).
48. Wang, K. *et al.* An Imaging Model Incorporating Ultrasonic Transducer Properties for Three-Dimensional Optoacoustic Tomography. *IEEE Trans. Med. Imaging* **30**, 203–214 (2011).
49. Kruger, R. A., Reinecke, D. R. & Kruger, G. A. Thermoacoustic computed tomography–technical considerations. *Med. Phys.* **26**, 1832–1837 (1999).
50. Xu, M., Xu, Y. & Wang, L. V. Time-domain reconstruction algorithms and numerical simulations for thermoacoustic tomography in various geometries. *IEEE Trans. Biomed. Eng.* **50**, 1086–1099 (2003).
51. Makarkin, M. & Bratashov, D. State-of-the-Art Approaches for Image Deconvolution Problems, including Modern Deep Learning Architectures. *Micromachines* **12**, 1558 (2021).
52. Manwar, R., Zafar, M. & Xu, Q. Signal and image processing in biomedical photoacoustic imaging: a review. *Optics* **2**, 1–24 (2020).
53. Cox, B. T., Laufer, J. G., Beard, P. C. & Arridge, S. R. Quantitative spectroscopic photoacoustic imaging: a review. *J. Biomed. Opt.* **17**, 61202 (2012).
54. Bulgarelli, B. & D'Alimonte, D. Chapter 4.1 - Simulation of In Situ Visible Radiometric Measurements. in *Optical Radiometry for Ocean Climate Measurements* (eds. Zibordi, G., Donlon, C. J. & Parr, A. C. B. T.-E. M. in the P. S.) vol. 47 407–449 (Academic Press, 2014).
55. Tarvainen, T. *Computational Methods for Light Transport in Optical Tomography (Laskennalliset menetelmät valon etenemisen mallittamiseen optisessa tomografiassa)*. (Kuopion yliopisto, 2006).

56. Tarvainen, T., Vauhkonen, M., Kolehmainen, V. & Kaipio, J. P. Finite element model for the coupled radiative transfer equation and diffusion approximation. *Int. J. Numer. Methods Eng.* **65**, 383–405 (2006).
57. Arridge, S. R. Optical tomography in medical imaging. *Inverse Probl.* **15**, R41–R93 (1999).
58. Schweiger, M., Arridge, S. R. & Nissilä, I. Gauss–Newton method for image reconstruction in diffuse optical tomography. *Phys. Med. Biol.* **50**, 2365 (2005).
59. Schoonover, R. W. & Anastasio, M. A. Image reconstruction in photoacoustic tomography involving layered acoustic media. *J. Opt. Soc. Am. A* **28**, 1114–1120 (2011).
60. Ammari, H., Bretin, E., Jugnon, V. & Wahab, A. Photoacoustic imaging for attenuating acoustic media. in *Mathematical modeling in biomedical imaging II* 57–84 (Springer, 2012).
61. Xu, Y. & Wang, L. V. Effects of acoustic heterogeneity in breast thermoacoustic tomography. *IEEE Trans. Ultrason. Ferroelectr. Freq. Control* **50**, 1134–1146 (2003).
62. Telenkov, S. & Mandelis, A. Signal-to-noise analysis of biomedical photoacoustic measurements in time and frequency domains. *Rev. Sci. Instrum.* **81**, 124901 (2010).
63. Zhou, M., Xia, H., Zhong, H., Zhang, J. & Gao, F. A noise reduction method for photoacoustic imaging in vivo based on EMD and conditional mutual information. *IEEE Photonics J.* **11**, 1–10 (2019).
64. You, K. & Choi, H. Inter-stage output voltage amplitude improvement circuit integrated with class-b transmit voltage amplifier for mobile ultrasound machines. *Sensors* **20**, 6244 (2020).
65. Stephanian, B., Graham, M. T., Hou, H. & Bell, M. A. L. Additive noise models for photoacoustic spatial coherence theory. *Biomed. Opt. Express* **9**, 5566–5582 (2018).
66. Aunon, J. I., McGillem, C. D. & Childers, D. G. Signal processing in evoked potential research: averaging and modeling. *Crit. Rev. Bioeng.* **5**, 323–367 (1981).
67. Butterworth, S. On the Theory of Filter Amplifiers. *Experimental Wireless and the Wireless Engineer* vol. 7 536–541 at (1930).
68. https://en.wikipedia.org/wiki/File:LowPass3poleICauer.svg.